ELSEVIER

Journal of Fluids and Structures 18 (2003) 771–781

JOURNAL OF FLUIDS AND STRUCTURES

www.elsevier.nl/locate/jnlabr/yjfls

Spurious counts in gas volume flow measurements by means of turbine meters

P.W. Stoltenkamp[a,*], S.B. Araujo[a], H.J. Riezebos[b], J.P. Mulder[b], A. Hirschberg[a]

[a] *Fluid Dynamics Laboratory, Department of Applied Physics, Technische Universiteit Eindhoven, Building Cascade, P.O. Box 513, Eindhoven 5600 MB, Netherlands*

[b] *Gasunie Research, N.V. Nederlandse Gasunie, Energieweg 17, 9743 AN Groningen, Netherlands*

Received 3 March 2003; accepted 12 August 2003

Abstract

Acoustical oscillations can induce a rotation of a turbine flow meter in the absence of main flow, which leads to spurious counts. A simplified model is presented which explains the occurrence of spurious counts in the limit of very thin turbine blades and high Strouhal numbers. The predicted threshold for the occurrence of spurious counts is compared to experimentally obtained data at various gas pressures in the range from 1 to 8 bar. The simplified model provides a reasonable prediction of the occurrence of spurious counts and can be used as an useful engineering tool in the prediction of the occurrence of spurious counts.

1. Introduction

Turbine flow meters are often used to measure volume gas flows in gas transport systems. These turbine flow meters are placed in a measurement manifold, consisting of several runs. Flow pulsations in these manifolds affect the accuracy of the flow turbine meters. The N.V. Nederlandse Gasunie (the Dutch gas authority) discovered that these pulsations not only affect turbine meters in open pipes, but can also incidentally cause spurious counts in turbine meters placed in a closed side branch in which there is no main flow. These spurious counts start above a certain critical pulsation level. Spurious counts that occur in open pipes, where a mean flow velocity is present has been studied by several authors (Cheesewright et al., 1996; McKee, 1992; Grenier, 1991; Dijstelbergen, 1966). The aim of the research is to obtain a better understanding of spurious counts under conditions for which there is no main flow. A simplified theoretical model is presented which explains the occurrence of these spurious counts in the limit of very thin turbine blades. The predicted threshold for the occurrence of spurious counts is compared to experimental data at various gas pressures in the range from 1 to 8 bar.

2. Theory

The spurious count behavior of a turbine meter can be explained by considering the forces acting on an aerofoil in an oscillating flow. The blades of the turbine rotor used in these gas transport systems have a rounded leading edge and a sharp trailing edge (see Fig. 1). This asymmetry causes the rotation.

*Corresponding author. Fax: +31-40-246-4151.

E-mail address: p.w.stoltenkamp@tue.nl (P.W. Stoltenkamp).

0889-9746/$ - see front matter
doi:10.1016/j.jfluidstructs.2003.08.019

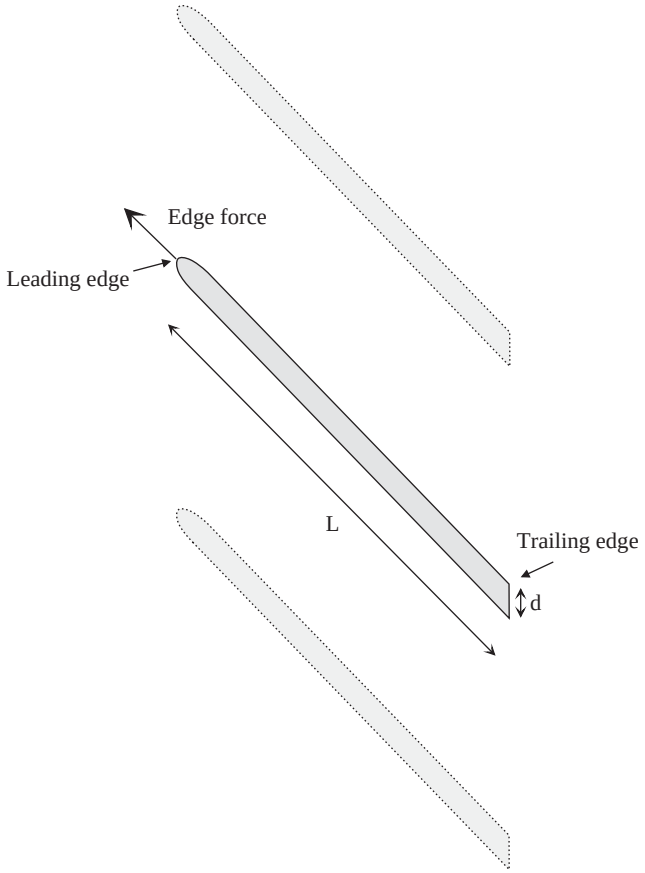

Fig. 1. Blades of the rotor.

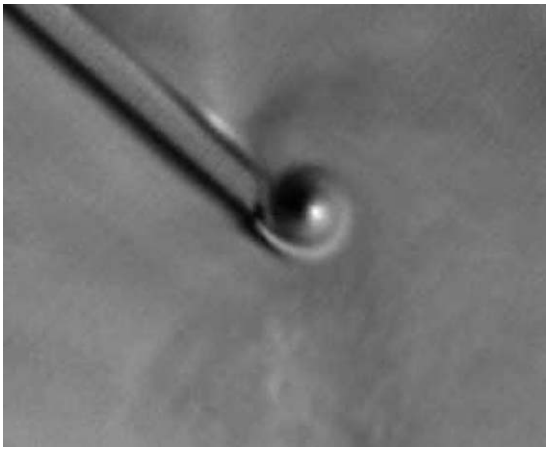

Fig. 2. Schlieren visualizations of the flow separation at the sharp edge at a Strouhal number, $Sr = \mathcal{O}(1)$.

In our model it is assumed that there is only flow separation around the sharp trailing edge of the blade. The flow separation at the sharp edge in an oscillating flow can be seen in schlieren visualizations (see Fig. 2).

Centrifugal forces in a potential flow around the edge of a plate cause a low pressure at the wall, which results in a force directed along the plate, which will be called the edge force. The vortex shedding reduces this edge force at the

sharp edge, while at the rounded edge it remains present. This leads to a net force on the blade. This force brings about a torque on the rotor. Spurious counts start when this torque is large enough to compensate the torque of the static friction forces.

This analysis is restricted to the case of a harmonic acoustical oscillation with frequency f (Hz) and amplitude U_{ac} ($\mathrm{m\,s^{-1}}$) of the particle velocity: $u' = U_{ac}\cos(2\pi ft)$. Furthermore, the turbine is considered under the condition that it does not yet rotate, so that the blades have a fixed position.

Important dimensionless numbers for this problem are the Helmholtz number, $\mathrm{He} = fd/c$, the Strouhal number, $\mathrm{Sr} = fd/U_{ac}$, the Reynolds number, $\mathrm{Re} = U_{ac}d/\nu$ and the ratio, d/L, of the thickness, d, of the blade compared with the length, L; ν is the kinematic velocity ($\mathrm{m^2\,s^{-1}}$) and c the propagation speed of sound waves ($\mathrm{m\,s^{-1}}$).

It is assumed that the viscous layer can be considered as a thin boundary layer ($Re \gg 1$). Hence, the flow around a blade of the turbine meter can be described with boundary layer theory in combination with potential flow theory. The flow is assumed to be locally incompressible, because the rotor is small compared to the acoustical wave length and the amplitude, U_{ac}, is small compared to the speed of sound ($He << 1$ and $M = U_{ac}/c << 1$). The Strouhal number, Sr_d gives an indication of the blade thickness compared to the acoustical displacement of particles.

If the product $\mathrm{Sr}_L = \mathrm{Sr}_d L/d$ is small, the blade thickness is small compared to the acoustical particle displacement and the flow can be assumed to be quasi-steady. If the Strouhal number is of order unity, $\mathrm{Sr}_d = \mathcal{O}(1)$ with $d/L << 1$, local vortex shedding occurs. Finally, if the Strouhal number is much larger than unity, $\mathrm{Sr}_d \gg 1$, vortex shedding is negligible except for the case when $d/L << 1$. This is illustrated in Fig. 3.

The ratio, d/L, of the thickness of the blade compared to the length, is small, $d/L = \mathcal{O}(10^{-1})$. In this theory, the blade is modelled as a flat plate. The flow separation at the sharp edge is modelled by means of a single-point vortex and by applying the Kutta condition at the sharp edge (also called Kutta–Joukowski condition). This corresponds to the model of Brown and Michael (1954) for flow separation at the edge of a delta wing. The force on the blade is found by integration of the pressure along the plate. The singular flow around the sharp leading edge results in a finite so-called edge force which is the result of an infinite low pressure applied on a zero surface (Milne-Thomson, 1952). A second model is considered for the limit case, where the Strouhal number is very large, $\mathrm{Sr}_d \gg 1$. Here a potential flow is considered without flow separation, but the contribution of the sharp trailing edge to the net hydrodynamic force on the blade is removed. The idea is that the vortex shedding at this sharp edge has removed the local flow singularity without affecting the global flow around the blade.

2.1. *Theory for the case* $\mathrm{Sr}_L(L/d) = \mathcal{O}(1)$

The theory for the case where the Strouhal number is order unity is considered first. In a point vortex model, the vortex sheet generated by flow separation at the sharp edge is represented by a single-point vortex. The vortex is assumed to be connected with the sharp edge of the plate by means of a feeding sheet. The circulation of the point vortex is calculated by applying the Kutta condition at the sharp edge. The Kutta condition requires the velocity to be finite at the sharp edge. In a real flow, this means that the flow leaves the edge tangentially, accounting for viscous effects. In a point vortex model, this implies that at the edge a stagnation point is assumed. The point vortex moves with the flow. Application of the Kutta condition implies then that the circulation changes with time. The convection

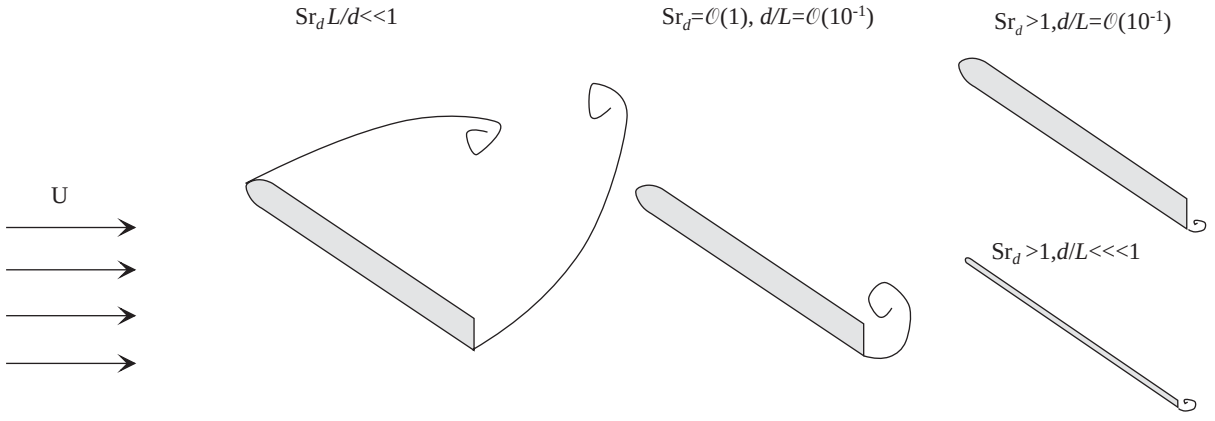

Fig. 3. Influence of Strouhal number and blade length to thickness ratio L/d on the flow.

velocity of the point vortex is calculated by means of potential flow theory. In this case a free vortex is assumed. This assumption is in contradiction with the time dependence of the circulation of the vortex. This induces a spurious force that will be neglected further (Rott, 1956). This error will appear not to be critical for our results.

The flow potential is calculated using a complex potential and conformal mapping. A circle with radius A, in the ξ-plane, is transformed in a flat plate of length $L = 4A$ in the z-plane using the transformation of Joukowski:

$$z = \xi + \frac{A^2}{\xi}, \tag{1}$$

where α is the incidence angle of the flow with respect to the blade (see Fig. 4).

The complex potential of the flow, Φ, in the transformed plane can now be written as

$$\Phi = U_{ac}\xi e^{-i\alpha} + \frac{U_{ac}A^2}{\xi}e^{i\alpha} - \frac{i\Gamma_v}{2\pi}\ln(\xi - \xi_v) + \frac{i\Gamma_v}{2\pi}\ln\left(\xi - \frac{A^2\xi_v}{|\xi_v|^2}\right). \tag{2}$$

The first and the second terms on the right-hand side are the acoustic flow potential, after applying the Milne-Thomson circle theorem (Milne-Thomson, 1952). The third and the fourth terms are the contributions of the vortex. Here ξ_v is the position of the vortex in the transformed plane and Γ_v the circulation of the vortex. The circulation of the vortex is calculated using the Kutta condition:

$$\left.\frac{d\Phi}{d\xi}\right|_{\xi=A} = 0. \tag{3}$$

At the first step the vortex is shed, the position of this vortex is calculated using the self-similar solution given by Howe (1975) for an impulsively starting flow around a semi-infinite plate. The velocity of the vortex, U_v, is calculated in the following steps using the following equation, assuming the vortex is a free vortex:

$$U_v^* = \frac{dz_v^*}{dt} = \left.\frac{d\Phi}{dz}\right|_{z=z_v} \lim_{\xi\to\xi_v}\left[\frac{d\Phi}{d\xi} + \frac{i\Gamma_v}{2\pi(\xi - \xi_v)}\right] \Big/ \frac{dz}{d\xi} + \frac{i\Gamma_v}{2\pi}\frac{d^2z}{d\xi^2} \Big/ \left(\frac{dz}{d\xi}\right)^2,$$

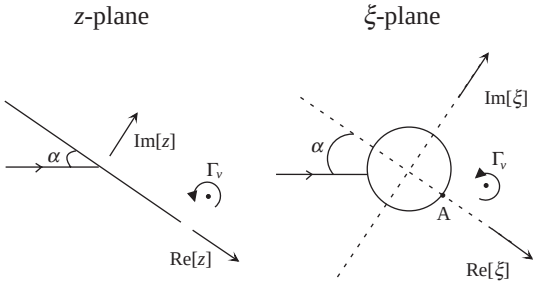

Fig. 4. Flat plate in the z-plane and ξ-plane.

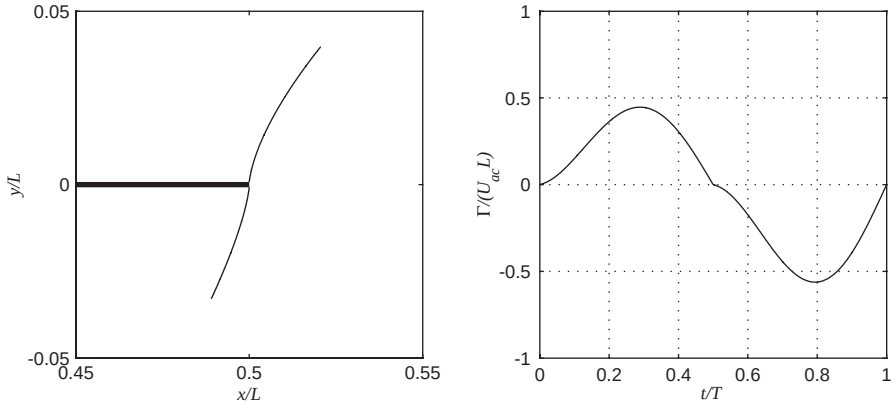

Fig. 5. (a) Calculated path of a single point vortex and (b) calculated vortex strength for $\mathrm{Sr}_L = 9$.

where z_v is the position of the vortex, ξ_v the position of the vortex in the transformed plane, the asterisk indicates the complex conjugate, Φ the complex potential and Γ_v the circulation of the vortex. The last term is known as the Routh correction (Clements, 1973). The new position of the vortex is calculated using a fourth-order Runge–Kutta integration scheme (Hirsch, 1988). The new circulation, Γ_v, of the vortex corresponding to this new position, is calculated using the Kutta condition (Eq. (3)). In this model the circulation of the vortex vanishes when the acoustic flow is zero. At the next time step a new vortex is shed. As an example the path of a single point vortex and its circulation is plotted in Fig. 5 for a typical case, where spurious counts were measured.

To calculate the torque on the turbine, the force on each blade is calculated numerically by integration of the pressure along the plate,

$$F = \oint p \, \mathrm{d}S = \int_{\text{without edge}} p \, \mathrm{d}S + \int_{\text{edge}} p \, \mathrm{d}S, \tag{4}$$

where p is the pressure (Pa) and S the surface area (m^2). The pressure, p, in the first term is solved using the unsteady Bernoulli equation,

$$\rho \frac{\partial \Phi}{\partial t} + \frac{1}{2}\rho u^2 + p = \text{constant}. \tag{5}$$

The integration is carried out by means of the trapezium method. For the second term, around the singularity, a quasi-steady approximation is used (Milne-Thomson, 1952 and Appendix A). As input for this theory, a Taylor expansion of Φ around the point $\xi = -A$ is used.

2.2. Limit of the theory for $\mathrm{Sr}_L = \mathrm{Sr}_d(L/d) \gg 1$

The limit of this theoretical model is considered next for $\mathrm{Sr}_L \gg 1$. In such a case the effect of the vortex on the global flow around the blade is negligible except for the flow near the sharp trailing edge. A great advantage of this simplified model is that an explicit expression is obtained for the aerodynamic torque on the rotor without the need to determine the details of the vortex path. As explained above, the key of this model is that it is assumed that there is only flow separation around the sharp trailing edge of the flat plate. As a consequence, there is a finite velocity at this sharp edge and therefore no edge force. At the leading, rounded edge there is no flow separation and the velocity becomes infinite and this results in an edge force (Fig. 6).

Because the velocity becomes infinitely large at the edge, convective flow acceleration is larger than the local time-dependent flow acceleration. A quasi-steady approximation can be used. The edge force is directed along the plate and can be calculated with potential flow theory (Milne-Thomson, 1952). The magnitude, F_e, of the edge force is

$$F_e = -\pi \rho S_{\text{plate}} U_{ac}^2 \sin^2 \alpha, \tag{6}$$

where F_e is the edge force (N), S_{plate} is the surface area of the plate (m^2), U_{ac} is the acoustic velocity amplitude ($\mathrm{m\,s^{-1}}$) and α is the angle between the blades and the direction of the acoustical flow. The flow separation generates a vortex close to the sharp edge. As explained above, this vortex is assumed to have solely the effect of removing the pressure singularity and the consequent edge force. Flow separation also implies that the boundary layer vorticity is injected into the main flow. This vorticity is assumed to be of small magnitude and confined to a region close to the edge; therefore, there will be no significant change of the global circulation for the flow around the flat plate. If the flat plate is placed in a parallel harmonic oscillating flow, the flow will alternate between the left and right situation in Fig. 6. The force perpendicular to the flat plate will also alternate harmonically. If a harmonically oscillating flow is imposed, the average of the normal force taken over one oscillating period will be zero. Consequently, the resultant averaged force for the flat plate over one acoustic period can be simply calculated using the edge force. With this edge force, it is possible to calculate the average torque, T_{av}, on the blades:

$$T_{av} = \frac{\pi \rho r_{av} S_{\text{plate}}}{8} U_{ac}^2 \sin^3 \alpha, \tag{7}$$

where r_{av} is the average radius (m) at which the force is applied on the blade.

2.3. Comparison models

In Fig. 7 the relative difference, $(T_1 - T_2)/T_2$ between the critical torque, T_1, calculated with the point vortex model for $\mathrm{Sr}_L = \mathcal{O}(1)$ and the critical torque, T_2, calculated with the model for the limit case $\mathrm{Sr}_L \gg 1$ is plotted against the reciprocal Strouhal number, $1/\mathrm{Sr}_L = U_{ac}/fL$, based on the length of the plate. For typical Strouhal numbers as

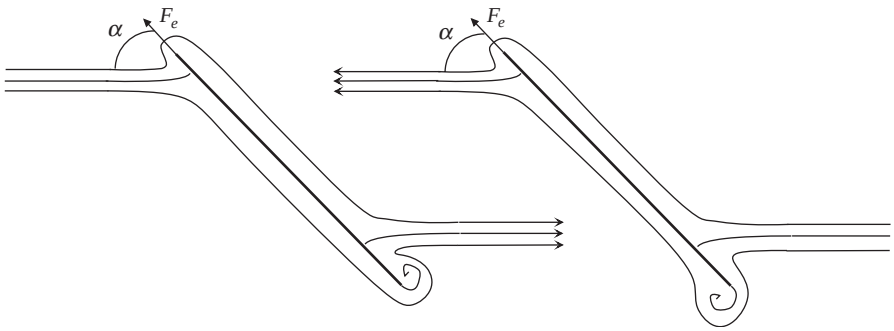

Fig. 6. Flow separation at the sharp edge for a flat plate in an oscillating flow.

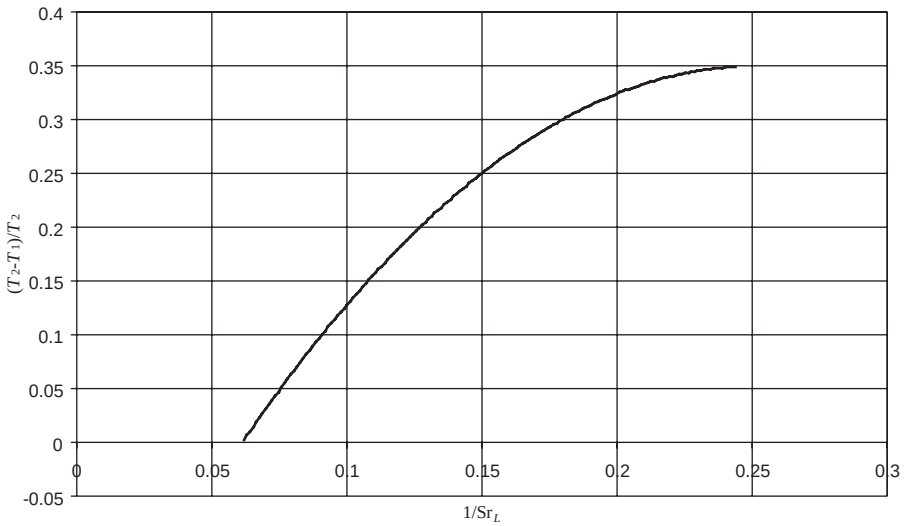

Fig. 7. The difference $(T_1 - T_2)/T_2$ between the critical torque calculated with the two models plotted against the reciprocal Strouhal number.

encountered in our experiments ($4 < \mathrm{Sr}_L \leq 20$) the difference between the two theories is less than 30% which is negligible compared to the difference between theory and experiments.

3. Experimental set-up

Acoustical oscillations in a closed side branch can either be induced by a resonant response to compressor pulsations or by flow-induced pulsations due to vortex shedding. In the experimental set-up, these flow oscillations are induced using a loudspeaker mounted within a closed pipe segment (Fig. 8).

Two set-ups were used (Mulder, 2000), a small set-up at atmospheric pressure with a pipe diameter $D = 100$ mm, and a large set-up, with a pipe diameter $D = 300$ mm and the possibility to vary the mean static pressure from 1 to 8 bar. In the small set-up, the gas turbine meter (Instromet G250) is placed between two PVC pipes with diameter $D = 100$ mm and length $L_{p1} = L_{p2} = 1.8$ m. A loudspeaker (Visaton W100S) is placed at the end of the pipe, while the other end is closed by a rigid plate. Four dynamical piezo-electric pressure transducers (Kistler type 7031) are placed at positions distributed along the pipes. The pressure transducers are connected to charge amplifiers (Brüel & Kjaer type 2635). In the large set-up, the gas turbine meter (Instromet G2500) is connected with two pipes with diameter $D = 300$ mm and lengths of $L_{p1} = 6$ m and $L_{p2} = 2$ m. The end of each pipe is sealed to be able to support a pressure up to 8 bar above atmospheric pressure. In the long pipe, L_{p1}, a loudspeaker (Peerless XLS10) is placed. The short pipe, L_{p2}, is closed by

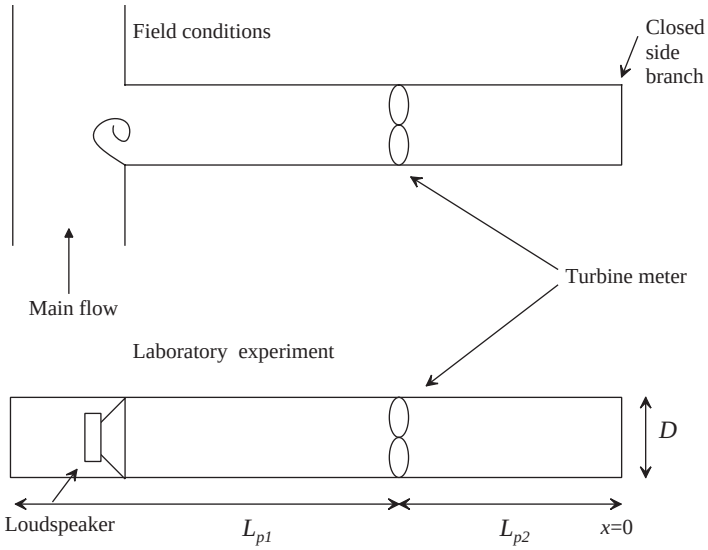

Fig. 8. Field conditions compared with experimental set-up.

means of a flat and rigid plate. The position of the loudspeaker can be changed, making it possible to modify the resonance frequency of the system. Nine holes are made for placing dynamical pressure transducers (Kistler type 7031) along the pipes, allowing an optimisation of the choice of the position of the four available transducers.

To obtain a harmonic voltage signal, a signal generator (LMS Roadrunner) is connected to a power amplifier (Brüel & Kjaer type 2706) from which the signal is applied to the loudspeaker. The amplitude and the frequency can be adjusted separately. For the acquisition of all the signals, a 12-channel data acquisition device (LMS Roadrunner compact) is used. The rotational frequency of the blades is measured using standard Instromet measuring equipment.

The pressure transducers are used to measure the acoustic pressure amplitude. As the acoustic waves in the pipe are plane waves, the pulsation pressure amplitude, $p'(x,t)$, depends only on the axis parallel to the pipe. This can be assumed if the frequency, f, of the pulsations is much smaller than the cut-off frequency, f_c. The pressure amplitude data is used to calculate the acoustic velocity amplitude, U_{ac}, if a full reflection at the closed end wall is assumed and thermal and friction losses in the pipe are neglected. The acoustic velocity at a distance x from the end of the wall is calculated using the equation

$$|u(x)| = \frac{|p'|}{\rho_0 c_0} \frac{\sin kx}{\cos k(x_m)}, \tag{8}$$

where $|u|$ is the acoustic velocity amplitude ($\mathrm{m\,s^{-1}}$), $|p'|$ is the acoustic pressure amplitude measured at a distance x_m (Pa), ρ_0 is the density of the propagation medium at ambient temperature ($\mathrm{kg\,m^{-3}}$), $c_0 \approx 344\ \mathrm{m\,s^{-1}}$ is the acoustical wave propagation velocity in air at ambient temperature ($\mathrm{m\,s^{-1}}$), k is the wave number ($\mathrm{m^{-1}}$) and x_m is the distance between the end wall of the pipe and the pressure transducer (m). To obtain the acoustic velocity, U_{ac}, at the blades of the turbine flow meter, incompressibility is assumed and from the mass conservation equation the following is obtained:

$$U_{ac} = |u(L_{p2})| \frac{S_m}{S_t}, \tag{9}$$

where U_{ac} is the amplitude of the acoustic velocity at the turbine blades ($\mathrm{m\,s^{-1}}$), L_{p2} is the pipe length (m) (see Fig. 8), $S_m = \pi D^2/4$ is the surface area of the pipe where the measurement is taken ($\mathrm{m^2}$) and S_t is the cross-sectional surface area of the turbine flow meter ($\mathrm{m^2}$). The flow through the turbine meter can be assumed incompressible, because the length of the turbine meter, L_t, is very small compared to the wave length, λ ($L_t << \lambda$). The frontal area of the blades of the turbine meter, which is about 10% of the internal area of the turbine meter, is neglected in calculating S_t. We used the values $S_t = 5.7 \times 10^{-3}\ \mathrm{m^2}$ for the small meter (Instrometer G250) and $S_t = 4.9 \times 10^{-2}\ \mathrm{m^2}$ for the large meter (Instromet G2500). Measurements of U_{ac} obtained from the four different pressure transducers agree with each other within 10%.

4. Experiments

4.1. Critical friction torque

Two different experiments are carried out to obtain the critical static torque above which rotation occurs: a dynamic and a static experiments. The equation of motion for the turbine flow meter is

$$I\frac{d\Omega}{dt} = T_{aer} + T_{fr}\,, \tag{10}$$

where I is the moment of inertia of the rotor relative to its axis (kg m^{-2}), Ω is the angular velocity (rad s^{-1}), t the time (s), T_{aer} is the aerodynamic torque at the blades of the rotor (kg m^{2}s^{-2}) and T_{fr} the total friction torque (kg m^2 s^{-2}). The aerodynamic torque is approximated in the previous section (see Eq. (7)).

The torque caused by the friction can be split into the contribution of air friction, T_{air}, on the rotor and in the torque caused by the friction, $T_{bearing}$, at the bearing (the friction with the oil and the friction of the shaft). The friction of the shaft can be divided in static friction or dynamic friction.

To obtain the torque of the dynamic friction, the rotor is accelerated by means of an acoustic field to a steady velocity. When the loudspeaker is turned off, the angular frequency decay is registered and a fourth-order curve is fitted through the data. Subsequently, the torque is calculated from the angular velocity using the relation in Eq. (10). The aerodynamic torque, T_{aer} is assumed to have a second-order dependency on the angular velocity (see Eq. (6)). The friction torque of the oil at the bearing has a linear dependency on the rotational velocity . The friction with the shaft is assumed to be constant. In the limit of vanishing rotational speed, the only contribution to the torque is the constant dynamic friction of the rotor with the shaft. The value of this dynamic torque is found by taking this limit to be approximately 6×10^{-6} N m for the small set-up and 9×10^{-5} N m for the large set-up.

The static friction torque is measured using a small piece of tape fixed at a known radius at the rotor. The tape induces a torque on the rotor, which can be calculated from the weight and the position of the tape. The rotor is held and released using a photograph shooter. With this method the critical static torque was found to be 5.6×10^{-6} N m for the small set-up and 1.0×10^{-4} N m for the large apparatus. These critical static torques agree within the experimental accuracy with the dynamic friction torques in the limit of zero rotational speed. Furthermore, these results agree with the specifications of the manufacturer.

4.2. Critical acoustic velocity

Above a critical value of the amplitude of the acoustic velocity, U_{ac}, spurious counts occur. This critical acoustic velocity is measured, by keeping the acoustical excitation frequency, f, constant, while increasing the amplitude slowly. This can be done either manually or by using a special function on the signal generator. When the rotor starts to rotate, the acoustic velocity is determined from the acoustic pressure amplitude, p', as explained in the previous section. These results show considerable deviations for different frequencies, but also for two consecutive measurements at the same frequencies. The standard deviation is approximately 20% of the mean value. Probable reasons for these deviations can be the varying static friction torque caused by the unevenly distributed oil and local roughness of the solid surfaces in the bearing. It is also possible that they are caused by changes that occur in flow configuration or by difficulties in determination of the threshold of rotation from the experimental data. The mean critical acoustic velocities are determined for the small and the large set-ups at their first and third resonance mode. For the small set-up these frequencies are $f_1 = 60$ Hz and $f_3 = 210$ Hz, and for the large set-up $f_1 = 30$ Hz and $f_3 = 100$ Hz. The critical acoustic velocity amplitude, U_{ac}, for the large set-up is measured at four different static pressures, 1, 2, 4 and 8 bar.

5. Results

The results of the experiments can now be compared to the calculated data and to the value of the critical pressure amplitudes in field conditions.

Fig. 9 shows the critical Strouhal number, $\mathrm{Sr}_d = df/U_{ac}$, based on the blade thickness, at which the rotation starts, plotted against the Reynolds number, based on the blade length. The critical Strouhal number is of order unity, which corresponds to our qualitative model of the effect of the blade thickness. When the vortex remains at distances from the edge smaller than the blade thickness, it is not expected that this affects the flow. Hence there is no rotation for $\mathrm{Sr}_d \gg 1$. A significant dependency of Sr_d on the Reynolds number can be observed, which we cannot explain with the used model. We did actually not expect such a dependency.

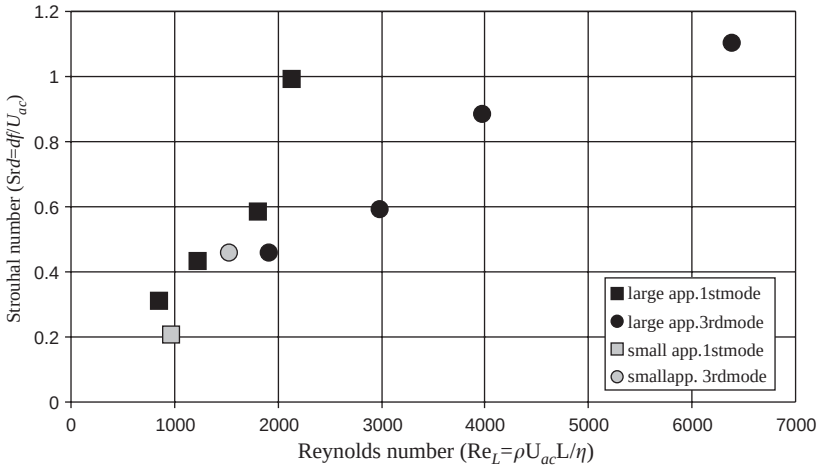

Fig. 9. The critical Strouhal number plotted against the Reynolds number.

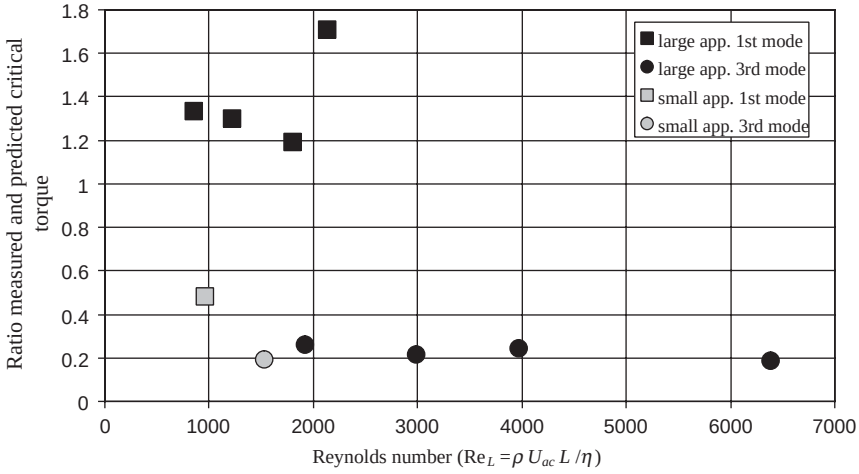

Fig. 10. The ratio between the measured critical torque and the calculated critical torque plotted against the Reynolds number.

In Fig. 10, the ratio of the measured critical static torque and the predicted torque calculated using the limit case model ($\mathrm{Sr}_L \gg 1$) for both set-ups is plotted against the Reynolds number, with the length of the blade as the characteristic length. For the small set-up, the calculated critical torque is two times the measured critical torque for the first resonance mode and five times the measured critical torque for the third mode. For the large set-up, the calculated critical torque is 20% lower than measured for the first mode and 4–5 times larger for the third mode. It would be interesting to investigate whether those differences in behavior for the first and third acoustical mode of the pipe are related to difference in mechanical vibration level. Such vibrations could affect the critical torque.

Using the results, the critical torque can be estimated for field conditions of natural gas transportation with a static pressure, $p = 60\,\mathrm{bar} = 6 \times 10^6\,\mathrm{Pa}$ and a density of the natural gas, $\rho_g = 14\,\mathrm{kg\,m^{-3}}$. The geometries of the pipe and of the turbine flow meter are assumed to be similar to that of the large set-up. Using Eq. (7) the acoustical velocity, U_{ac}, is calculated, at which the critical static torque is reached and spurious counts occur. This is found to be $U_{ac} \approx 7 \times 10^{-2}\,\mathrm{m\,s^{-1}}$. This corresponds to acoustical pressure amplitudes of the order of $p' = \rho_0 c_0 U_{ac} \approx 10^3$ Pa with for natural gas $c_0 \approx 390\,\mathrm{m\,s^{-1}}$. In field conditions, measurements show spurious counts with acoustic pressure amplitudes of 4×10^3 Pa (Riezebos et al., 2001). This shows that the model can provide a fair indication for conditions for the occurrence of spurious counts.

6. Conclusions

Representing the rotor blade by a flat plate and the flow separation at the sharp edge of the blade by a point vortex, a model is obtained allowing to predict the aerodynamic torque on the rotor. A simplified model is proposed for high Strouhal number ($Sr_L >> 1$) which provides an explicit algebraic expression without the need to determine the details of the flow. Comparison between the two models indicates that they are equivalent within the accuracy of the performed experiments. The results show that the thickness of the plate is an important factor for occurrence of spurious counts. The presence of a thick trailing edge on turbine blades increases the critical acoustical pulsation amplitude above which spurious counts appear. The model provides a prediction of the order of magnitude of the critical torque, and can be used to determine typical conditions for the occurrence of spurious counts in field conditions. In view of its simplicity, the simplified model for the limit case, $Sr_L >> 1$, is an useful engineering tool in the prediction of the occurrence of spurious counts.

Acknowledgements

The authors like to thank Remi Zorge, Freek van Uittert, Jan Küchel and Arjan Hamelinck for their contribution to the flow visualization. This research is financially supported by the technology foundation STW (STW project *Flow-Induced Pulsations in Gas Transport Systems*).

Appendix A

Using the transformation of Joukowski (see Eq. (1)), the value of $d\xi/dz$ can be calculated close to the leading (singular) edge,

$$\lim_{z\to -2A}\left[\frac{d\xi}{dz}\right] = \lim_{z\to -2A}\left[\frac{1}{2}+\frac{z}{2\sqrt{(z-2A)(z+2A)}}\right] = \lim_{z\to -2A}\frac{i\sqrt{A}}{2\sqrt{z+2A}}, \tag{A.1}$$

where A is the radius of the circle in the ξ-plane. Because near the edge ($z\to -2A$) becomes very large and the second term becomes the dominant term, Eq. (A.1) is obtained. The potential of the flow is given by Eq. (2). With this equation and the Kutta condition on the trailing edge, $z = 2A$ (see Eq. (3)) the circulation, Γ_v, can be found

$$\Gamma_v = 4\pi U_{ac}\sin\alpha\frac{A(A-\xi_v)(\xi_v^*-A)}{\xi_v\xi_v^*-A^2}, \tag{A.2}$$

where U_{ac} is the acoustic oscillation amplitude, α is the incidence angle of the flow and ξ_v is the position of the vortex in the transformed plane. Using the flow potential, Φ and the circulation Γ_v, $d\Phi/d\xi$ close to the leading edge can be calculated:

$$\begin{aligned}\left[\frac{d\Phi}{d\xi}\right]_{\xi\to -A} &= U_{ac}e^{-i\alpha} - U_{ac}e^{i\alpha} - \frac{i\Gamma_v}{2\pi}\left(\frac{1}{-A-\xi_v}+\frac{\xi_v^*}{-A\xi_v^*-A^2}\right)\\ &= -2iU_{ac}\sin\alpha\left(1+\frac{(A-\xi_v)(A-\xi_v^*)}{(A+\xi_v)(A+\xi_v^*)}\right).\end{aligned} \tag{A.3}$$

By combining Eqs. (A.1) and (A.3) it follows that

$$\begin{aligned}\left[\frac{d\Phi}{dz}\right]_{z\to -2A} &= \left[\frac{d\Phi}{d\xi}\right]_{\xi\to -A}\left[\frac{d\xi}{dz}\right]_{z\to -2A}\\ &= U_{ac}\sqrt{A}\sin\alpha\left(1+\frac{(A-\xi_v)(A-\xi_v^*)}{(A+\xi_v)(A+\xi_v^*)}\right)\frac{1}{\sqrt{z+2A}}.\end{aligned} \tag{A.4}$$

The force on the edge can be found by evaluating Blasius theorema around the closed contour ε,

$$F_x - iF_y = \frac{i\rho}{2}\lim_{\varepsilon\to 0}\oint_\varepsilon\left(\frac{d\Phi(z)}{dz}\right)^2 dz, \tag{A.5}$$

where F_x represents the force parallel to the plate (the edge force) and F_y represents the force perpendicular to the plate.

Using the Cauchy integral theorem, the force becomes

$$F_x = F_e = -\pi\rho U_{ac}^2 A\sin^2\alpha\left(1+\frac{(A-\xi_v)(A-\xi_v^*)}{(A+\xi_v)(A+\xi_v^*)}\right)^2$$
$$= -4\pi\rho U_{ac}^2 A\sin^2\alpha\left(\frac{A^2+\xi_v\xi_v^*}{(A+\xi_v)(A+\xi_v^*)}\right)^2. \quad \text{(A.6)}$$

References

Brown, C.E., Michael, W.H., 1954. Effect of leading-edge separation on the lift of a delta wing. Journal of the Aeronautical Sciences 21, 690–694.

Cheesewright, R., Atkinson, K.N., Clark, C., Horst, G.J.P., Mottram, R.C., Viljeer, J., 1996. Field Tests of Correction Procedures for Turbine Flowmeters in Pulsatile Flows. Flow Measurement and Instrumentation 7, 7–17.

Clements, R.R., 1973. An inviscid model of two-dimensional vortex shedding. Journal of Fluid Mechanics 57, 321–336.

Dijstelbergen, H.H., 1966. Dynamic Response of Turbine Flowmeters. Instrument Review 13, 241–245.

Grenier, P., 1991. Effects of Unsteady Phenomena on Flow Metering. Flow Measurement and Instrumentation 2, 74–80.

Hirsch, C., 1988. Numerical Computations of Internal and External Flow, Vol. I. Wiley, Chichester.

Howe, M.S., 1975. Contribution to the theory of aerodynamic sound, with application to excess jet noise and the theory of the flute. Journal of Fluid Mechanics 71, 625–673.

McKee, R.J., 1992. Pulsation Effects on Single- and Two-rotor Turbine Meters. Flow Measurement and Instrumentation 3, 151–166.

Milne-Thomson, L.M., 1952. Theoretical Aerodynamics. MacMillan & Co., London.

Mulder, J.P., 2000. Ontwerp en bouw van een resonator ten behoeve van onderzoek naar pulsatiegevoeligheid van turbinegasmeters. Internal Report N.V. Nederlandse Gasunie, ART.2000.R.0592., Groningen.

Riezebos, H.J., Mulder, J.P., Zwart, R., 2001. Influence of flow pulsations on turbine flow meters. In: Proceedings of the Eighth International Gas Research Conference, Amsterdam.

Rott, N., 1956. Diffraction of a weak shock with vortex generation. Journal of Fluid Mechanics 1, 111–123.